

<https://doi.org/10.1038/s41612-024-00607-3>

Assessing hydrothermal changes in the upper Yellow River Basin amidst permafrost degradation

Check for updates

Lei Song^{1,2,3}, Lei Wang^{1,2}✉, Dongliang Luo⁴, Deliang Chen⁵ & Jing Zhou¹

Since the 20th century, the temperature on the Qinghai–Tibetan Plateau (QTP) has increased at a rate of 2–3 times that of global warming. Consequently, the soil temperature and active layer thickness have also increased, which have directly caused severe degradation of the frozen ground on the QTP. Using a hydrological model driven by climate and vegetation forcing, the spatial and temporal changes in the hydrothermal characteristics of the Upper Yellow River Basin (UYRB) from 1960 to 2019 were modeled and the mechanism of the changes was analyzed. During the past six decades, the soil temperature in the UYRB exhibited an increasing trend. The degradation of permafrost in the UYRB was accompanied by thickening of the active layer, a reduction of the maximum depth of the seasonal frost penetration, and continuous extension of the basin thawing time. This degradation was also associated with the increase in the soil moisture content and decrease in the soil ice content, resulting in degradation of the permafrost area by one-tenth of the total area in the UYRB. The reduction of the permafrost area and the thickening of the active layer can profoundly impact hydrological processes and ecosystems. These findings play a critical role in designing efficient strategies to manage and protect frozen ground and serve as a valuable reference for understanding the consequences of frozen ground degradation globally.

The cryosphere, which encompasses glaciers, frozen ground, snow, and various forms of ice, is one of the most vulnerable spheres of the Earth to human activities and climate change^{1,2}. The frozen ground consists of permafrost and seasonally frozen ground. Here, permafrost refers to the soil layers where the soil temperature is below 0 °C for more than two consecutive years^{3,4}, and seasonally frozen ground usually freezes and thaws annually in areas without permafrost or with a deep permafrost table⁵. Permafrost covers 20% of the land area in the Northern Hemisphere, while seasonally frozen ground (including the active layer above the permafrost) covers approximately 56%⁶. In recent years, there has been a significant focus on the correlation between frozen ground and global climate change. The Qinghai–Tibetan Plateau (QTP), which is the most prominent high-altitude region globally^{7,8}, reacts more positively to climate warming than the high-latitude permafrost area in the Arctic^{9,10}. Since the 1980s, the permafrost cover on the QTP has decreased by a total of $0.45 \times 10^6 \text{ km}^2$ (ref. 11). Permafrost degradation on the QTP has altered the hydraulic connection

between the surface water resources and soil moisture not only in time but also in space. As a distinctive regional water barrier or weakly permeable layer^{12,13}, frozen ground degradation limits physical processes such as water vapor exchange between the atmosphere and the soil. Therefore, it is of great importance to comprehensively summarize the dynamic characteristics and regulations pertaining to frozen ground on the QTP. This reveals the complex and multilayered interactions that arise under climate warming conditions.

Frozen ground significantly affects engineering, ecology, and water security in arid regions^{14–16}. Climate change has intensified the impact of permafrost degradation¹⁷. Research indicates that permafrost loss on the QTP could lead to the expansion of lakes¹⁸. Moreover, intensified thawing of permafrost will disrupt the water–heat balance on the QTP and will consequently generate thermokarst lakes¹⁹. Ice-marginal landforms destroy the integrity of the land surface to some extent, further exacerbating the degradation of fragile ecosystems in cold and arid regions and the process of

¹State Key Laboratory of Tibetan Plateau Earth System, Environment and Resources (TPESER), Institute of Tibetan Plateau Research, Chinese Academy of Sciences, 100101 Beijing, China. ²University of Chinese Academy of Sciences, Beijing, China. ³PIESAT Information Technology Co., Ltd, Beijing, People's Republic of China. ⁴State Key Laboratory of Frozen Soil Engineering, Northwest Institute of Eco-Environment and Resources, Chinese Academy of Sciences, Lanzhou, China. ⁵Department of Earth Sciences, University of Gothenburg, Box 46, S-405 30 Gothenburg, Sweden. ✉e-mail: wanglei@itpcas.ac.cn

desertification²⁰. Additionally, thickening of the active layer for many years will lead to the release of organic materials previously sequestered in the ground and flowing with the groundwater, further accelerating global warming. It has been emphasized that in the future, permafrost degradation on the QTP may form a vast carbon source^{21,22}, and large amounts of CO₂, CH₄, and other gases will be released into the atmosphere²³, which will further affect the regional carbon cycle and meteorological conditions^{24,25}.

In summary, the degradation of frozen ground fundamentally alters the processes of surface and groundwater storage and movement, which further affects the geological conditions. Furthermore, it also partially affects processes such as the water containment function and atmospheric circulation^{26,27}. However, the poor representativeness and high uncertainty of cryospheric climate data, coupled with the limited observations of frozen ground, have led to unsophisticated analysis of the physical processes within the frozen ground in the cryosphere and have seriously hindered research on frozen ground degradation. Therefore, it is of great significance to reveal the trends and patterns of the changes in frozen ground to understand the changes in the physical processes in cold regions under climate warming. In-depth knowledge of the long-term evolution patterns of frozen ground, changes in the soil layer depth characteristics, and research on the effects of frozen ground on the land surface water cycle, ecosystems, and socio-economics is of great significance and application value for the ecological construction and protection of frozen ground.

The aim of this study was to examine the spatiotemporal changes in the hydrothermal characteristics of the permafrost in a large river basin on the QTP over the past 60 years by using a physically based distributed permafrost hydrology model from 1960 to 2019.

To achieve this paper's objectives, The Upper Yellow River Basin (UYRB) was chosen. It is located above the Tangnaihai hydrological station (Fig. 1a), and is an integral part of the Water Tower of Asia. The UYRB originates from the northern Bayan Har Mountains on the QTP²⁸ and has a total area of approximately $13.4 \times 10^4 \text{ km}^2$ ²⁹. The elevation of the terrain gradually decreases from west to east and from south to north, with a large elevation drop. The UYRB has a typical plateau continental climate³⁰, and the precipitation decreases from southeast to northwest. The average annual temperature is $-2.3 \text{ }^\circ\text{C}$, indicating an overall arid and cold climate³¹.

Additionally, the UYRB serves as a transition zone where seasonally frozen ground and permafrost intersect at high altitudes in the mid-latitude region (Fig. 1b)³². Seasonally frozen ground, sporadic permafrost, and predominantly continuous permafrost coexist in this basin, and the spatial distribution of the frozen ground is diverse and complex. Four mountain ranges in the basin contain frozen ground: the Bayan Har Mountains and the Anyemaqen Mountains in the upper reaches of the basin are mainly surrounded by permafrost, and the Xiqing Mountains and the Minshan Mountains in the southeastern part of the basin predominantly contain seasonally frozen ground. Furthermore, the study area contains two sister lakes, Gyaring and Ngöring lakes, located between the Bayan Har Mountains and the Buqing Mountains. The vegetation in the study area is predominantly alpine meadow and alpine steppe, followed by forest, steppe, and desert^{33–35}. The UYRB possesses a variety of complex geomorphological features and noticeable changes in the frozen ground, while the completeness of the meteorological and hydrological data and the abundance of permafrost observation data in this region make it one of the best regions for studying the formation and historical evolution of the frozen ground on the QTP³².

Results

Changes in soil hydrothermal conditions

To examine the current state of the frozen ground in the UYRB, in this paper, we employ simulation data from a hydrological model to evaluate the soil temperature, soil moisture, and ground ice. The western part of the UYRB is characterized by permafrost, while the eastern part is characterized by seasonally frozen ground. Based on the data presented in Fig. 2a, the soil temperatures at shallow (2 cm) and deep (200 cm) soil depths in the UYRB have exhibited a general increase in temperature since the 1960s. The rate of

increase of the temperature in the shallow soil was $0.17 \text{ }^\circ\text{C}/10\text{a}$, whereas that in the deep soil was $0.21 \text{ }^\circ\text{C}/10\text{a}$, indicating a consistent trend of increasing deep soil temperature in the UYRB. The data reveal that under identical climate change conditions, the deep soil temperature in the UYRB has maintained an increasing trend, and the rate of warming was higher than the increase in the shallow soil temperature, indicating that the frozen ground in this area has been continuously thawing. It is of particular importance to note that in 1986, the regional average soil temperature at a depth of 200 cm increased to above zero. Only 12 years later, in 1998, the regional average soil temperature at this depth increased by $1 \text{ }^\circ\text{C}$, which was similar to the increase in the air temperature. This suggests that the permafrost in the Uruguayan Frontier Zone was severely degraded and thawed under climate warming.

The soil temperature exhibited varying patterns over time. Specifically, from 1960 to 1979, the shallow soil temperature decreased even as the deep soil temperature increased; the soil temperatures at both depths increased from 1980 to 1999; and the shallow soil temperature decreased, while the deep soil temperature increased from 2000 to 2019. These results imply that there were considerable fluctuations in the changes in the shallow soil temperature. In addition to its close correlation with the air temperature, the shallow soil temperature was influenced by precipitation and other environmental factors, and the infiltration of water into the shallow soil formed interflow, which, in combination with the conspicuous process of shallow soil evapotranspiration, resulted in significant fluctuations of the shallow soil temperature.

According to the spatial variations in the shallow (2 cm) soil temperature (Fig. 3), the UYRB as a whole experienced warming during the past 60 years (Fig. 3e). During 1960–1979, the soil temperatures in the permafrost region decreased slightly, while the warming in the seasonally frozen ground region was insignificant (Fig. 3f), indicating that the permafrost was less affected by the air temperature during this period. However, from 1980 to 1999, the entire watershed experienced dramatic and sustained warming (Fig. 3g). In contrast, during 2000–2019, the warming rate slowed down and even exhibited a cooling trend in the permafrost region (Fig. 3h). Averaged over the entire watershed, the shallow soil temperature increased significantly in both the permafrost and seasonally frozen ground regions (Fig. 3a–d).

Regarding the spatial distribution of the deep (200 cm) soil temperature (Fig. 3), the trends of the deep soil temperature and shallow soil temperature remained consistent over the 60-year period. However, the increase in the deep soil temperature in the seasonally frozen ground region was significantly higher than that in the permafrost region. During the three consecutive periods, i.e., 1960–1979, 1980–1999, and 2000–2019, the entire watershed exhibited an increase in temperature in the seasonally frozen ground, as well as significant fluctuations in the permafrost near the Anyemaqen Mountains. The permafrost only warmed slightly, but the area above $0 \text{ }^\circ\text{C}$ gradually changed from scattered islands to continuous zones.

In conclusion, the UYRB as a whole underwent warming over the past six decades, and the seasonally frozen ground experienced more dramatic changes in response to climate warming than the permafrost. Although the soil temperatures continued to increase throughout the basin, the rate of surface soil temperatures decelerated after the 21st century. This implies that as the climate changes, permafrost will be affected in a more diverse pattern, with significant impacts on ecological and hydrological processes.

Furthermore, frozen ground has a major impact on the soil moisture and ground ice, as well as the soil temperature. The average ground ice content in the 0–200 cm soil layer within the UYRB decreased and the rate of change was $-0.002 \text{ m}^3\text{m}^{-3}/10\text{a}$ (Fig. 2b). Notably, around the onset of the 21st century, the average ground ice content exhibited a marked decline. Regarding the spatial distribution of the 0–200 cm soil moisture (Fig. 4), the mean soil moisture was larger in the southeast and interior parts of the basin, with a maximum value of $>0.37 \text{ m}^3\text{m}^{-3}$, while the mean soil moisture was lower in the western and northern parts of the basin, with a minimum value of $\sim 0.16 \text{ m}^3\text{m}^{-3}$. Furthermore, the mean soil moisture content at depths of 0–200 cm in the seasonally frozen ground region differed significantly from

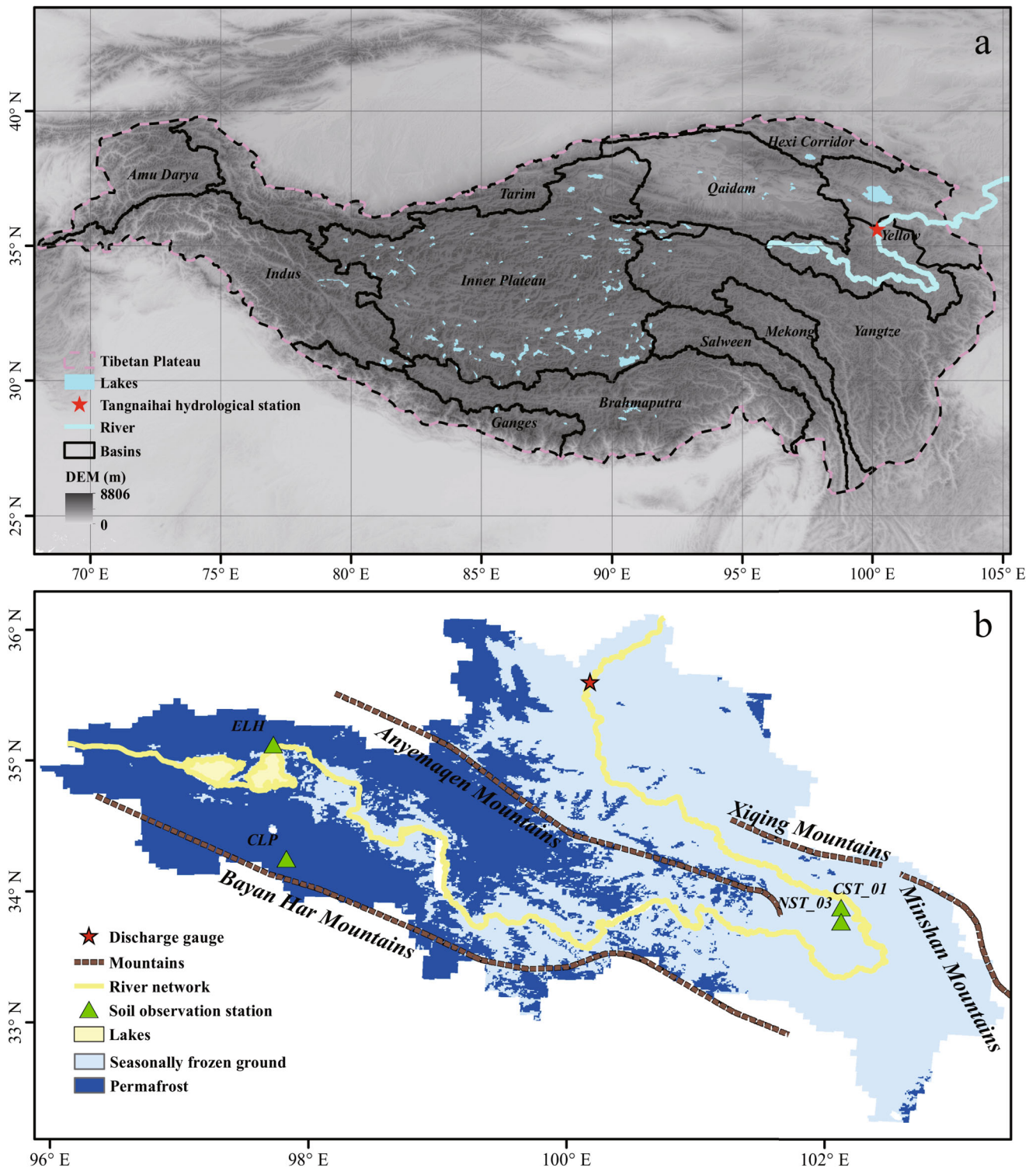


Fig. 1 | Geographic of the Upper Yellow River Basin (UYRB). a Tibetan Plateau DEM map and location of the UYRB; and **(b)** distribution of frozen ground in the UYRB.

the values in the permafrost region. Since the 1960s, the average soil moisture content has increased throughout the watershed. From 1960 to 1979, the average soil moisture content decreased slightly. Subsequently, the soil moisture content in the seasonally frozen ground region exhibited a weak increase, whereas the average soil moisture content in the permafrost region (near Gyaring and Ngöring) underwent a marked decline. Between 1980 and 1999, the soil experienced thawing, and the average soil moisture content increased gradually from southeast to northwest. From 2000 to 2019, the soil thawed rapidly throughout the source region, leading to a

marked increase in the average soil moisture content. These findings suggest that the permafrost in the UYRB degraded at a relatively slow rate in the 1980s and 1990s. Between 1980 and 1999, the soil experienced thawing, and the average soil moisture content increased gradually from southeast to northwest.

Figure 4 shows that the average ground ice content at depths of 0–200 cm in the eastern part of the UYRB and in the area surrounding the Sister Lakes (the Gyaring and Ngöring lakes) was low, with a minimum value of $0.03 \text{ m}^3 \text{ m}^{-3}$. In contrast, the western part of the UYRB had a high

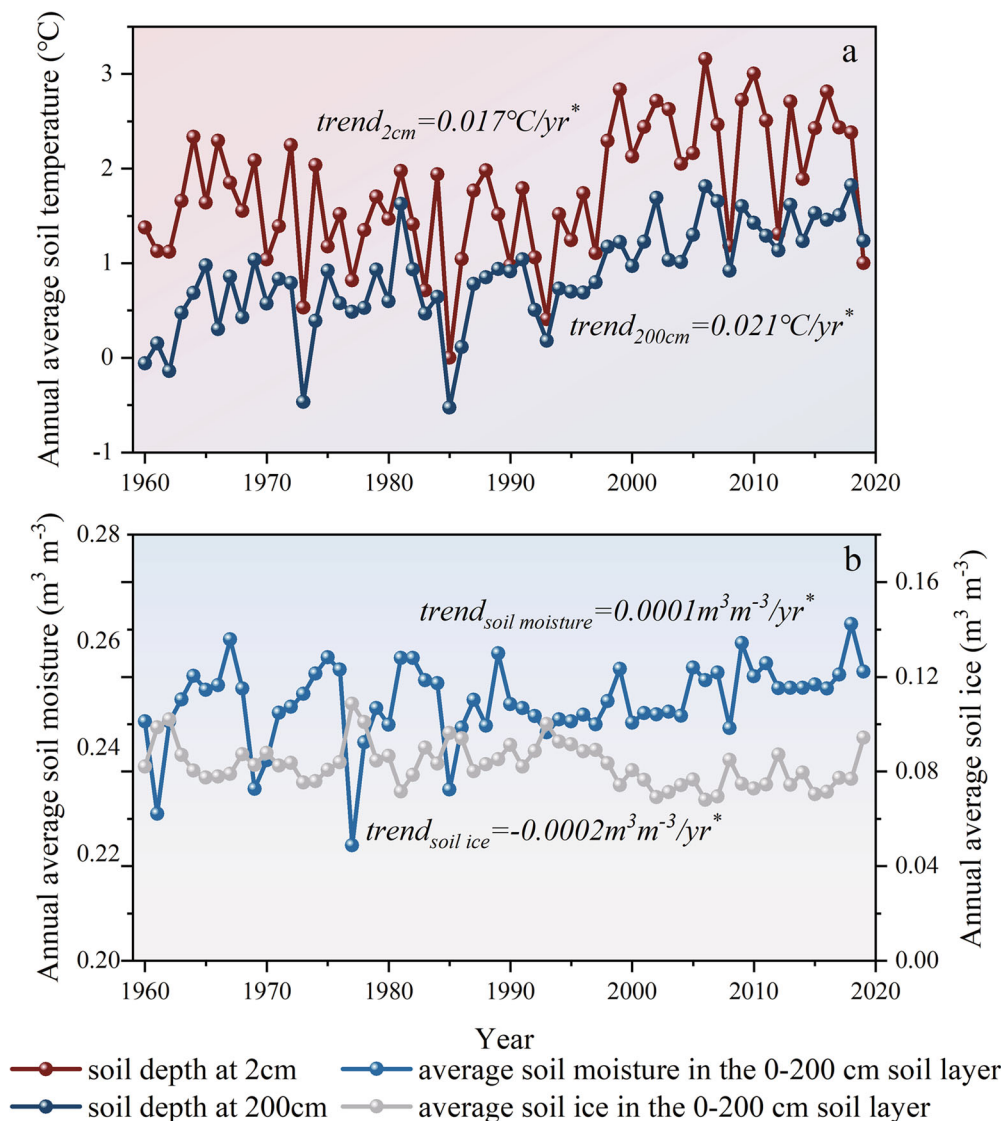


Fig. 2 | Hydrothermal trends in the Upper Yellow River Basin (UYRB). Simulated long-term changes in the (a) basin-averaged soil temperature at depths of 2 cm and 200 cm, and (b) mean soil moisture and soil ice content of the 0–200 cm soil layers. * denotes that the trend passes the significance test ($p < 0.05$).

ground ice content, with a maximum value of $0.24 m^3 m^{-3}$. The average ground ice content in the permafrost region was substantially greater than that in the seasonally frozen ground region. Although the overall average ground ice content exhibited a decreasing trend, there was a slight increase in the ground ice near the two mountain ranges (the Bayan Har Mountains and the Anyemaqen Mountains) in the permafrost region. Between 1960 and 1979, the average ground ice content in the northern part of the UYRB decreased gradually, but almost the entire basin exhibited an increasing trend. Moreover, between 1980 and 1999, the ground ice content decreased in most of the UYRB, but it noticeably increased in the interior parts. From 2000 to 2019, there was a decrease in the average ground ice content in the seasonally frozen ground region, whereas the permafrost region (west of Gyaring and Ngöring lakes) experienced an increasing trend.

Changes in the average ground ice content can occur for several reasons. First, heavier precipitation during the summer and spring (Supplementary Fig. 1) may result in the storage of more water in the active layer, leading to an increase in the amount of frozen water. Additionally, in permafrost regions, the surface soil temperatures are lower than the subsurface soil temperatures in winter, creating a temperature gradient that moves unfrozen water from the upward to the bottom of the active layer. During the summer, the temperature of the surface soil is higher than the

temperature of the soil beneath it. This causes a temperature gradient that is opposite to that in the winter. Additionally, a significant amount of liquid water moves downward. The temperature gradient during summer is much larger than that in winter, with a larger amount of water flowing downwards compared to the amount of water migrating upwards during winter. As the climate continues to warm, the summer temperature gradient strengthens, which may lead to increased downward migration of the soil moisture and the accumulation of frozen moisture at the bottom of the active layer.

Based on analysis of the temporal average ground ice content in the basin (Fig. 4i–l), it was found that the melting of the permafrost mainly occurred to the southeast of Sister Lakes. The permafrost in the UYRB is expected to gradually degrade and spread from south to northwest between the Bayan Har Mountains and the Anyemaqen Mountains toward the Sister Lakes. In summary, the decreasing ground ice content in the UYRB has led to an increase in the total amount of soil moisture, and the soil moisture also significantly increased from the 1980s to the 1990s, indicating that the permafrost in the UYRB started to degrade.

Permafrost distribution

Over the past 60 years (1960–2019), the UYRB has undergone significant changes in the soil temperature, soil moisture, and ground ice as a result of

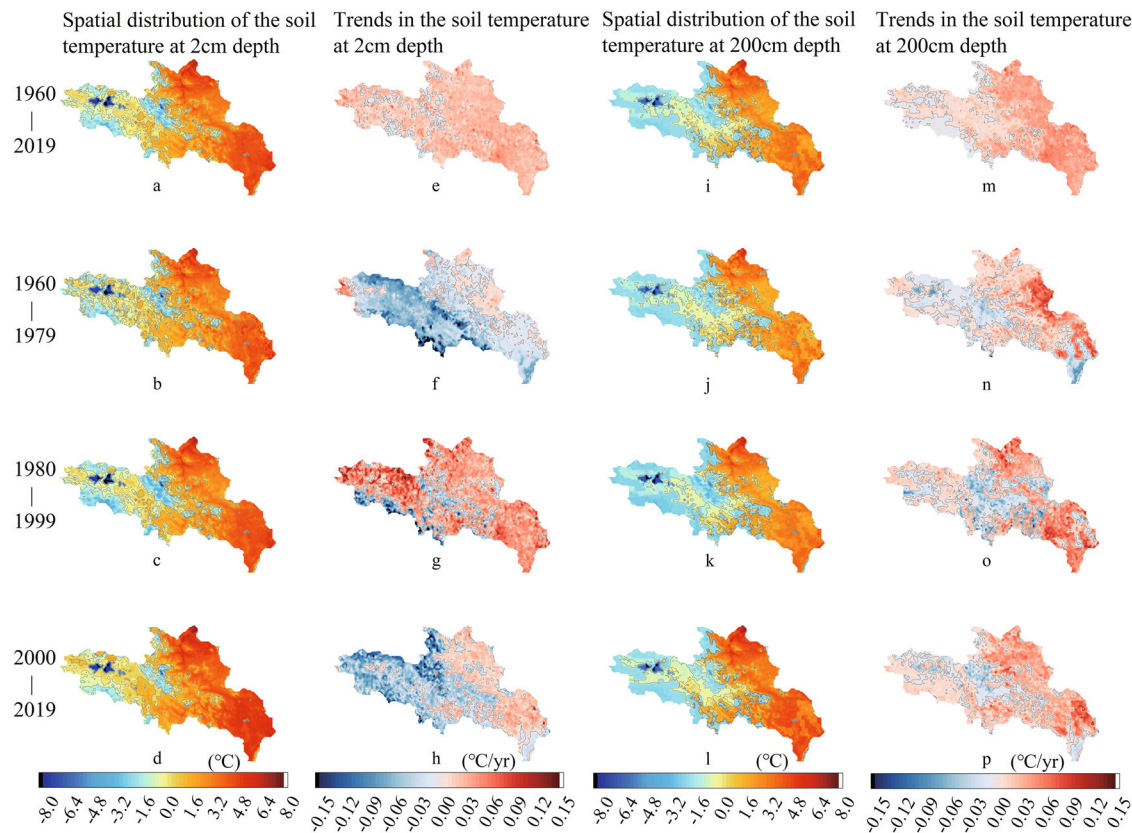


Fig. 3 | Soil temperature trends in the Upper Yellow River Basin (UYRB). a–d The spatial distribution of 2-cm soil temperatures for 1960–2019, 1960–1979, 1980–1999, 1999–2000. e–h The trends in the 2-cm soil temperature for 1960–2019, 1960–1979, 1980–1999, 1999–2000. i–l The spatial distribution of 200-cm soil temperatures for 1960–2019, 1960–1979, 1980–1999, 1999–2000. m–p The trends in the 200-cm soil temperature for 1960–2019, 1960–1979, 1980–1999, 1999–2000.

climate change. These changes have had a profound impact on permafrost formation, aggradation, and degradation in the watershed. During the 1960s and 1970s, there was a steady decrease in the area of the permafrost, especially in the Sister Lakes region, i.e., the southeastern part of the Gyaring and Ngöring lakes and the eastern part of the Bayan Har Mountains. However, in the 1980s and 1990s, the permafrost expanded again from sporadic permafrost to predominantly continuous permafrost in the southeastern region of the transition zone. Certain climatic factors may have caused the re-formation and expansion of the permafrost, which had a positive effect on the permafrost cover in the basin. After the beginning of the 21st century, the permafrost in the eastern part of the Bayan Har Mountains began to degrade again. Additionally, the sporadic and predominantly continuous permafrost in the hinterland of the basin gradually degraded and exhibited a discontinuous distribution. The occurrence of this degradation may have been related to the intensification of climate change and the influence of human activities. As the climate warms, the soil temperature in the UYRB rises, causing faster melting of the permafrost. Furthermore, anthropogenic activities such as land use change and water resource development may also have had some negative impacts on the degradation of the permafrost. Considering the degradation results for each period and excluding the bias of the model simulation effect, it can be concluded that the permafrost degradation in the UYRB has exhibited an accelerated trend under climate change during the past 60 years. Statistically, the permafrost area degraded at a rate of $-2143 \text{ km}^2/10 \text{ a}$, and the total permafrost degradation area accounted for 10.77% of the total basin area (Fig. 5).

Variations in freeze-thaw indicators

To achieve a more profound comprehension of the frozen ground trend in the UYRB, in this section, we divide the basin into permafrost and seasonally frozen ground regions and present a focused analysis. In this section, we focus on the following indicators of freezing and thawing: the active layer

thickness (ALT) of the permafrost, the maximum depth of the seasonal frost penetration (MFD) of the seasonally frozen ground, the start date of the shallow soil layer thawing, the end date of the shallow soil thawing (start of freezing), and the duration of the shallow soil thawing. The 60-year period is divided into six time periods (1960–1969, 1970–1979, 1980–1989, 1990–1999, 2000–2009, and 2010–2019) to enable comparative and analytical investigation of the present status and trend of the changes in the types of permafrost in the UYRB.

Figure 6 shows that there was a noticeable increase in the average ALT of the permafrost in the UYRB, with a rate of $0.015 \text{ m}/10\text{a}$. In the early 21st century, the ALT increased significantly, which was consistent with the change in the ground ice content. The onset of permafrost thawing shifted earlier at a rate of $-1.24 \text{ d}/10\text{a}$, whereas the beginning of the freezing was delayed at a rate of $0.59 \text{ d}/10\text{a}$. Additionally, the thawing period of the basin has lengthened by $1.83 \text{ d}/10\text{a}$. Since the 1960s, the duration of the permafrost thawing in the UYRB has increased, which increased the transfer of heat to the deeper soil layer, thus accelerating the degradation of the permafrost. The degradation and formation of permafrost are influenced by factors such as the air temperature, land surface temperature, precipitation, evaporation, geology, vegetation, and snow accumulation. Although the start, end, and duration of thawing are indicators of the degradation of permafrost, they have exhibited large inter-decadal differences.

Under the background of climate warming, the thawing period in the UYRB has increased and the freezing period has shortened in the permafrost region in the UYRB, which has led to more heat transfer to the deeper layers of the soil and accelerated the thawing process of the permafrost, thus contributing to thickening of the ALT. During the 1960s, the ALT increased from south to north. In particular, the ALT to the southeast of the Sister Lakes reached a maximum value of 2.87 m. In the 1970s, the area of the permafrost decreased and part of it became seasonally frozen ground in the area adjacent to the Sister Lakes. The distribution of the ALT remained

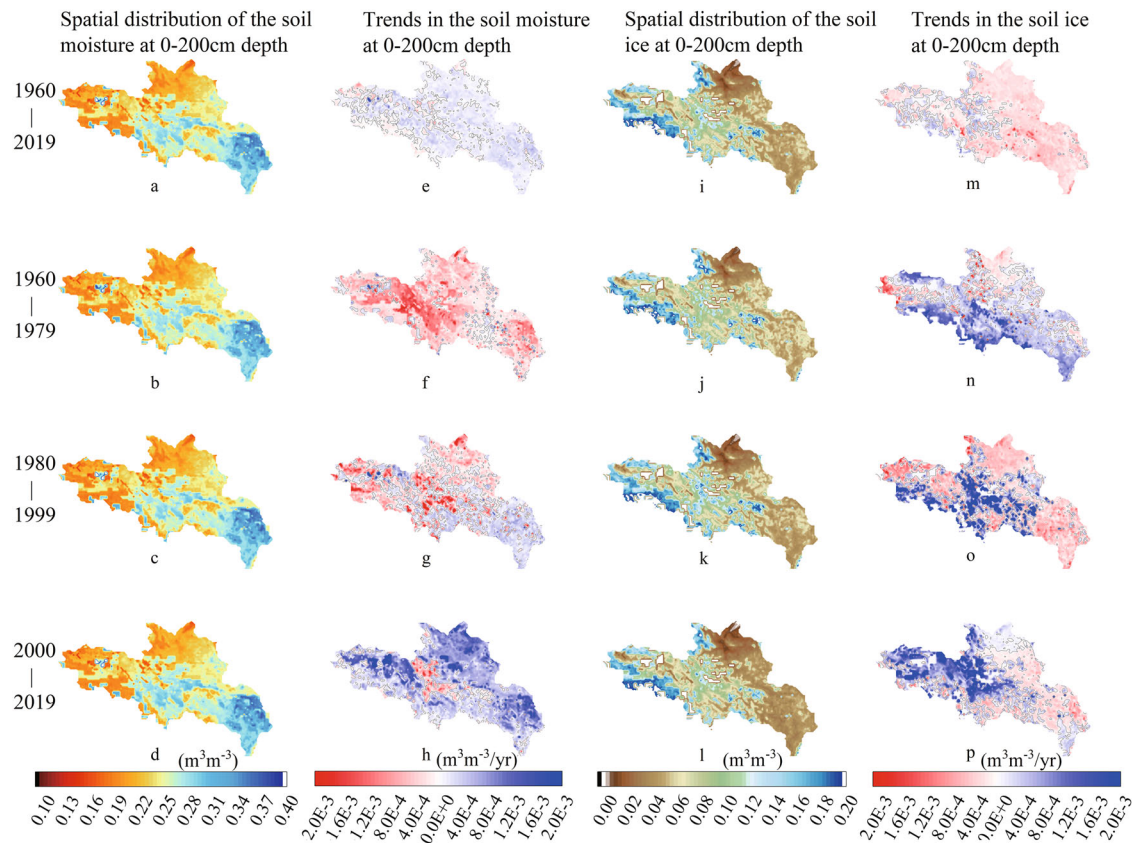


Fig. 4 | Changes in soil moisture and soil ice content in the UYRB from 1960 to 2019. a–d The spatial distribution of 0–200-cm soil moisture for 1960–2019, 1960–1979, 1980–1999, 1999–2000. e–h The trends in the 0–200-cm soil moisture for 1960–2019, 1960–1979, 1980–1999, 1999–2000. i–l The spatial distribution of 0–200-cm soil ice for 1960–2019, 1960–1979, 1980–1999, 1999–2000. m–p The trends in the 0–200-cm soil ice for 1960–2019, 1960–1979, 1980–1999, 1999–2000.

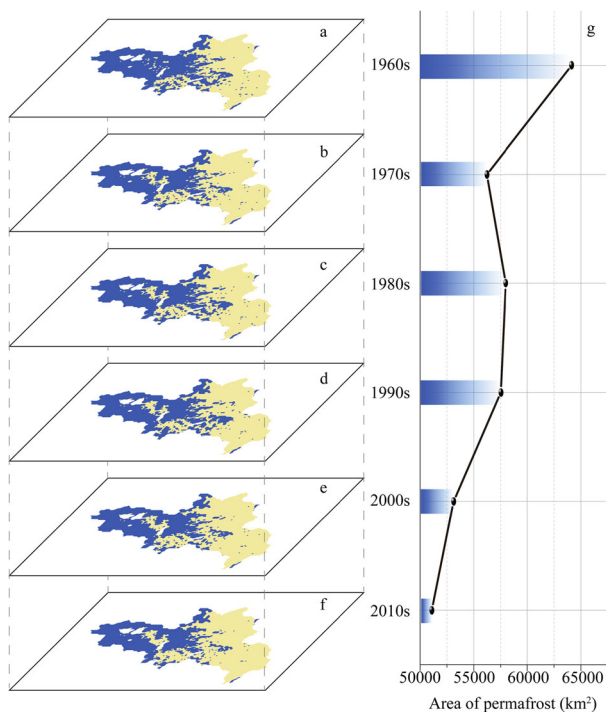


Fig. 5 | Changes in the area of permafrost in the UYRB from 1960 to 2019. a–f Distribution of the permafrost and seasonally frozen ground areas in 1960s, 1970s, 1980s, 1990s, 2000s, and 2010s. g Interannual changes in permafrost area from 1960 to 2019.

similar to that in the 1970s, with slight development near the Bayan Har Mountains and in the interior of the basin. The permafrost area and the ALT expanded again in the 1990s due to the combined effects of temperature and precipitation. This led to the development of permafrost near the Bayan Har Mountains and the Anyemaqen Mountains, and eventually led to a decrease in the ALT. The degradation of the permafrost in the hinterland led to a significant increase in the ALT in the early 21st century. The largest increase in the ALT occurred in the regions between the Anyemaqen Mountains and the Sister Lakes. From 2010 to 2019, the permafrost in the hinterland steadily decreased, whereas the ALT of the sheet permafrost decreased slightly (Fig. 7f). Overall, during the 60-year period, the ALT of the permafrost exhibited a generally increasing trend. This trend is mainly attributed to the sporadic permafrost in the interior of the UYRB and along the river channel in the direction of the Sister Lakes, as well as to the increase in the thickness in the vicinity of the Bayan Har Mountains and the Anyemaqen Mountains.

The changes in the seasonally frozen ground in the UYRB were highly significant (Fig. 6c). The MFD significantly decreased at a rate of $-0.075 \text{ m}/10\text{a}$, and the depth of the frozen ground was above 1.5 m predominantly before the 1990s (1960, 1961, 1973, and 1985). In the entire basin, the beginning and end dates of the thaw period, as well as the duration of the thaw period, exhibited significant changes overall. The onset of thawing occurred significantly earlier (at a rate of $-2.24 \text{ d}/10\text{a}$), the end of the thaw period was delayed significantly (at a rate of $1.60 \text{ d}/10\text{a}$), and the duration of the thawing season increased at a rate of $3.82 \text{ d}/10\text{a}$ (Fig. 6d). Generally, the thawing period in the seasonally frozen ground region was more pronounced and fluctuated less than that in the permafrost region.

The spatial variability of the MFD shown in Fig. 7h–m indicates that the changes in the seasonal frozen ground were more uniform than the changes in the permafrost. The MFD decreased during the 1960s and 1970s, and the deepest depth occurred on the southeastern side of the Sister Lakes.

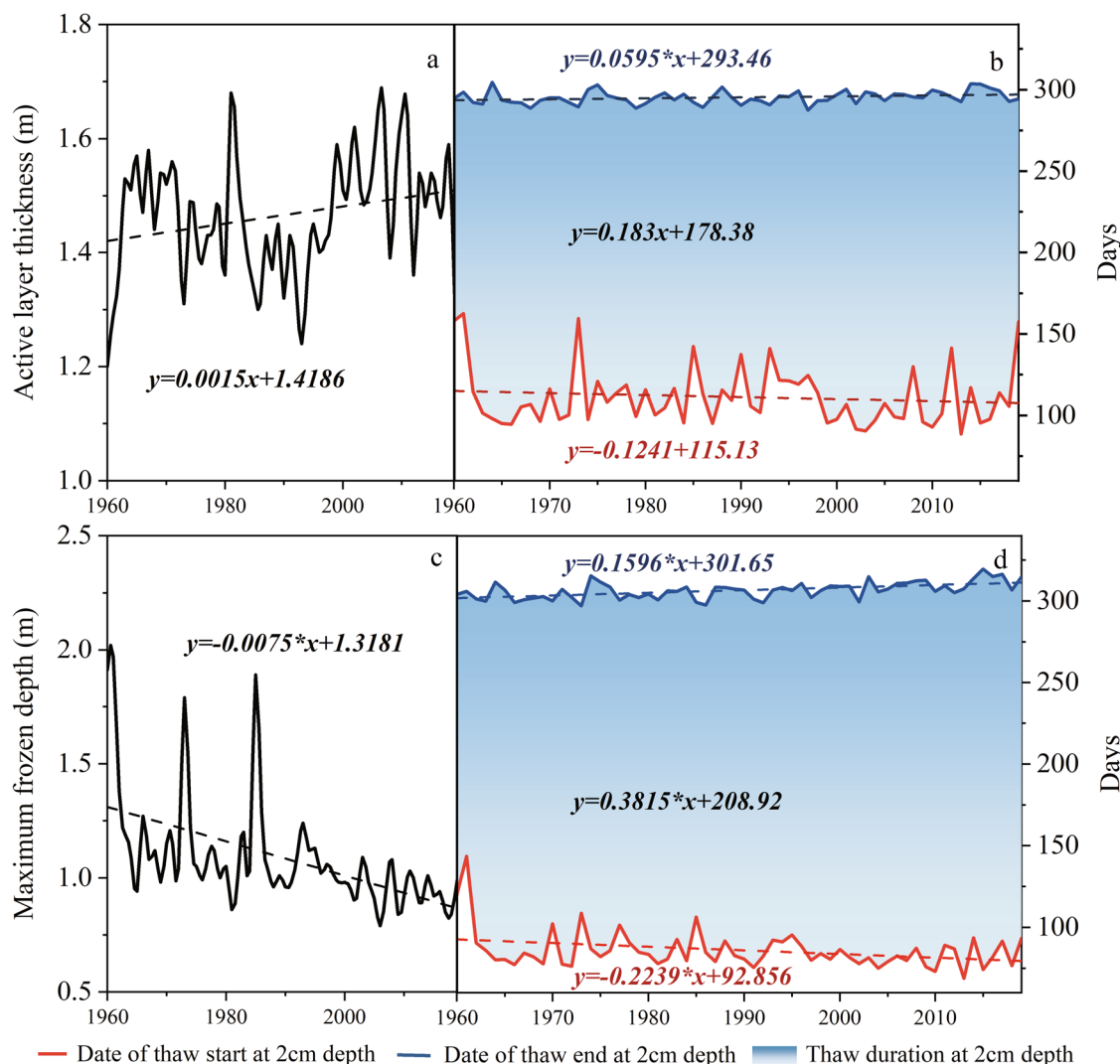


Fig. 6 | Variations in freeze-thaw indicators. Inter-annual variations in the (a) active layer thickness and the (c) maximum frozen depth; and the thawing period at a depth of 2 cm depth in the (b) permafrost and (d) seasonally frozen ground regions in the UYRB from 1960 to 2019. * denotes that the trend passes the significance test ($p < 0.05$).

The maximum MFD was mainly due to the fact that the seasonally frozen ground in this area was formed from permafrost degradation in the 1960s. However, during the 1980s, the seasonally frozen ground around the Tangnaihai hydrological station continued to thaw, causing the MFD to increase slightly in most of this area, and the range below 1 m became wider. In the 1990s, almost all of the seasonally frozen ground had an MFD of <1 m, except for near the Xiqing Mountains and the areas developed from permafrost. In the 21st century, near the Xiqing Mountains, the freezing depth of the seasonally frozen ground decreased to <1 m. This reduction occurred gradually and intensified over time throughout the entire seasonally frozen ground area. Through observation of the age-averaged distribution of the MFD, it is evident that the area with the previously profoundest MFD is now becoming shallower. This is indicative of the typical interdecadal process of the degradation of permafrost into seasonally frozen ground. Over the past 60 years, the MFD in the UYRB has exhibited a sustained decrease (Fig. 7n). The most notable reduction in the MFD, ranging from 0.4 to 0.6 m, occurred in the southeastern part of the basin during the 21st century. Furthermore, predictions based on the current conditions suggest that the degradation of the frozen ground in the UYRB will accelerate, and the seasonally the frozen ground in the southeastern corner will be the first to be converted to non-frozen ground.

The degradation of frozen ground was characterized not only by changes in the ALT and MFD but also by the complex physical process of

the thawing (or freezing) regime, which differed in terms of the start time, end time, and duration of the thawing period, and the different thawing cycles further affected the magnitude of degradation and the ability of the soil to store heat. In the 1960s (Fig. 8a, h), thawing began on the 110t–120th days in large areas of shallow soil in the upper part of the basin, while it occurred on the 80–90th days in the lower part of the basin. During the 1970s, the thawing time advanced in the upper area along the river channel and in the lower area of the basin, and the end time of the melting was gradually delayed in the vicinity of the Xiqing Mountains (Fig. 8b, i). In the 1980s and 1990s, the changes in the soil thawing were similar to those observed in the 1970s. However, it should be noted that while the thawing cycle was extended overall, the onset of thawing was delayed more significantly in the 1990s in the vicinity of the Bayan Har Mountains and the Anyemaqen Mountains. Beginning in the 21st century, the temperature of the soil in the basin shifted to 1.5 °C, which led to a large advance in the thawing of the permafrost zone, and the soil started to thaw almost 1 month earlier in total over the 60-year period (Fig. 8e, f). Additionally, the end of the thawing period was also largely delayed until after the 300th day and covered the entire seasonally frozen ground region (Fig. 8l, m). As a result, the start of the thawing period in the UYRB advanced and the corresponding end of the thawing period was delayed, which together contributed to the annual increase in the duration of the thawing period. Slightly opposite trends occurred in the vicinity of the Bayan Har Mountains and the Anyemaqen

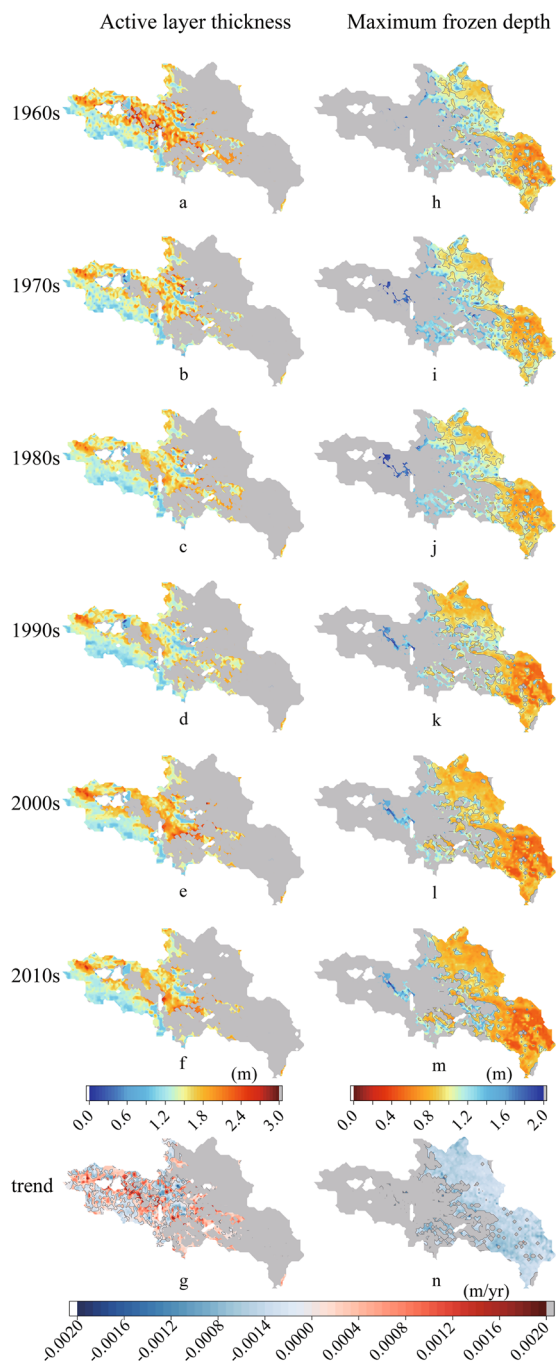


Fig. 7 | Changes in soil depth in the UYRB from 1960 to 2019. **a–f** The spatial distributions of the active layer thickness. **g** The trend of the active layer thickness. **h–m** The spatial distributions of the maximum frozen depth. **n** The trend of the maximum frozen depth.

Mountains (Fig. 8f, m, t). The extension of the duration of the thawing period also allowed the soil to absorb more heat, which promoted melting of the ground ice and the degradation of the permafrost.

Discussion

Focusing on the UYRB, which includes the basin above the Tangnaihai gauge in the Yellow River, we developed a permafrost physical parameterization scheme as a research tool to study hydrology in the cryosphere. Our analysis was based on the observational data from China Meteorological Administration (CMA) stations, Food and Agriculture Organization (FAO) soil type data, United States Geological Survey (USGS) land use data, and SOILGRID soil organic matter data. The objective was to

comprehensively analyze and reproduce the development and degradation process of the frozen ground in the UYRB during the past 60 years (1960–2019) in order to reveal the spatial and temporal characteristics of the frozen ground in the UYRB under climate warming on the QTP. It was found that the warming rates of the shallow and deep soil temperatures in the UYRB were 0.17 °C/10a and 0.21 °C/10a, respectively. It was also revealed that the average soil moisture (0–200 cm) increased slowly at a rate of 0.001 m³m⁻³/10a, and the soil ice content decreased at a rate of -0.002 m³m⁻³/10a. By analyzing the soil temperature changes, it was found that the permafrost area in the UYRB decreased by 13,050 km² during the past 60 years, accounting for 10.8% of the entire basin area. The ALT of the permafrost increased at a rate of 0.015 m/10a, the mean MFD of the seasonally frozen ground decreased significantly (-0.075 m/10a), and the duration of the thawing period of the frozen ground in the UYRB increased continuously (permafrost: 1.83 d/10a; seasonally frozen ground: 3.82 d/10a). The seasonally frozen ground responded more positively to warming than the permafrost degradation. Based on the current conditions, it is predicted that the frozen ground in the UYRB will degrade at an accelerated rate. It is expected that the seasonally frozen ground in the southeastern part of the study area will be the first region to degrade to non-frozen ground.

Furthermore, the duration of the permafrost thawing increased with global warming, releasing more soil moisture, and the temperature gradient within the soil forced the soil moisture to move upward. Moreover, this resulted in increased surface runoff generation and confluence, which in turn influenced the seasonal effects, long-term effects, and extreme surface runoff events³⁶.

Under global warming, the problem of the degradation of the frozen ground on the QTP is becoming increasingly serious. The hydrothermal-physical processes in the frozen ground region are specific and complex, with changing trends, and they have a significant impact on the regional hydrological and ecological processes. Due to the vastness of the QTP, its sparse population, and high altitude, meteorological-hydrological-frozen soil observations in many of the high-altitude permafrost regions are exceedingly uncommon. For instance, there is only one national meteorological station, Maduo Station, in the vicinity of the permafrost region in the upper reaches of the UYRB. Consequently, there is a substantial uncertainty in the regional climate change and permafrost degradation, as well as the evaluation of the role of permafrost in the hydrology of this region.

Hydrological model outputs and analyses are significantly limited by input data (e.g., climate forcing data, soil data, and vegetation data). As a result, complete observation data are urgently needed to drive the development of cryosphere research technologies. To reduce the uncertainty caused by insufficient meteorological station data and inadequate quality control, we suggest openly accessing and widely collecting hourly observation data from meteorological stations in the QTP region. After processing, these data can effectively replace the original input data of the model, thus improving the simulation accuracy. Geohydrological data from other regions of the world with similar altitude and climatic characteristics can be analyzed using various methods, such as linear fitting and machine learning, to optimize the soil and vegetation information for the QTP region. Simultaneously, input simulation experiments with a large number of samples and multiple sets of bias data should be conducted to reasonably verify the existing conclusions.

To explore and analyze the effects of changes in permafrost and seasonally frozen ground on hydrological-ecological processes, the majority of existing hydrological or land-surface models require improvement in terms of the physical processes. In frozen ground regions, the development and degradation of snow and glaciers also often occurs. This interacts with the atmosphere to generate extremely complex hydrological and ecological processes. In this study, we specifically examined the degradation characteristics of permafrost. However, when discussing the degradation mechanisms and its upstream and downstream impacts, it is essential to consider the interactions between the snowpack, permafrost, glacial processes, and ecological and climatic processes.

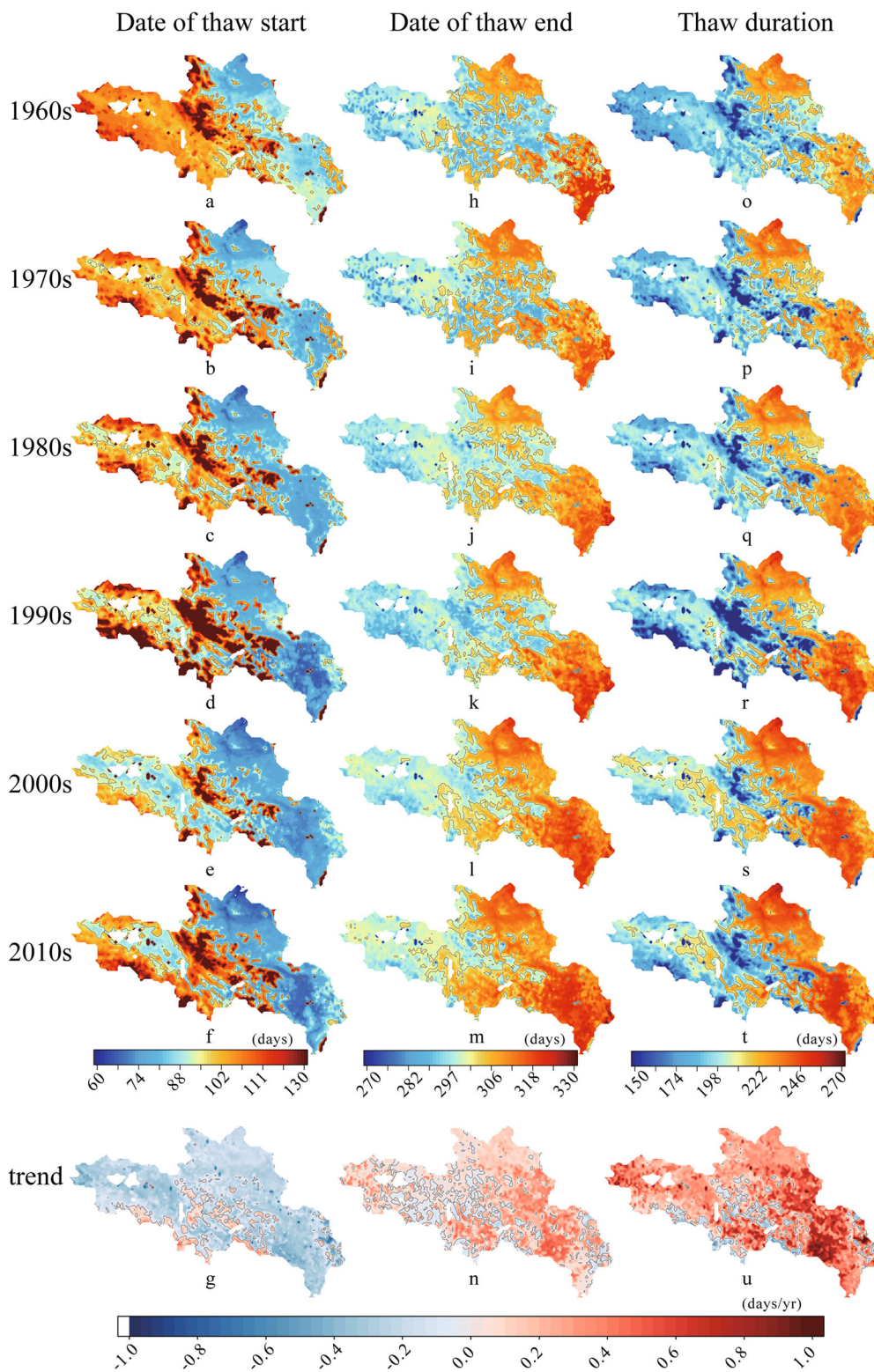


Fig. 8 | Changes in freeze–thaw times in the UYRB from 1960 to 2019. a–f The spatial distributions of the date of thaw start. g The trend of the date of thaw start. h–m The spatial distributions of the date of thaw end. n The trend of the date of thaw start. o–t The spatial distributions of the date of thaw duration. u The trend of the date of thaw duration.

Methods

Datasets

The datasets utilized in this study included four types of basic geographic data, remote sensing vegetation data, climate forcing data, and land surface observation data for the UYRB. These data were employed to construct,

drive, calibrate, and validate the accuracy of the permafrost hydrology model. The details regarding all aspects of the data used are described below.

(a) Basic geographic data

The basic geographic data for the UYRB included the following sources and content.

- Digital elevation model (DEM) data: Shuttle Radar Topography Mission (SRTM) data (<http://srtm.csi.cgiar.org/>) with a resolution of 90 m.
- Land use data: from the United States Geological Survey (USGS) database (<http://edc2.usgs.gov/glcc/glcc.php>) with a grid accuracy of 1 km.
- Soil type data: global digital soil dataset published by the FAO of the United Nations (<http://www.fao.org/geonetwork/srv/en/main.home>). This dataset has a spatial resolution of 5 km and provides data for soil depths, as well as various hydraulic parameters such as the saturated soil moisture content and soil anisotropy ratio.
- Soil organic carbon data: 1 km organic carbon data from the International Soil Reference and Information Center (ISRIC) (<https://soilgrids.org/>), including seven soil depth levels, 0 m, 0.05 m, 0.15 m, 0.30 m, 0.60 m, 1.00 m, and 2.00 m.

(b) Remote sensing vegetation data

To assess the influence of the dynamic vegetation alterations in the water resources, we utilized vegetation information obtained from the Global Land Surface Satellite Products System (GLASS)³⁷. This dataset has a spatial resolution of 0.25° and a temporal resolution of 8 days, providing the Land area index (LAI) and the fraction of the absorbed photosynthetically active radiation (FPAR). Both were used as the model's vegetation forcing data to participate in the computation of the land surface physical processes in the hydrological model.

(c) Climate forcing data

The daily meteorological data for the UYRB were acquired from daily observations made by the China Meteorological Administration (CMA, <https://data.cma.cn/en>) at twenty-two selected stations within and around the basin. The data include seven variables: downward shortwave radiation, downward longwave radiation, air pressure, water vapor pressure, air temperature, wind speed, and precipitation. The radiation data were calculated from the air pressure, temperature, humidity, sunshine duration, and wind speed data in the observation dataset using a hybrid model^{38,39}.

(d) In situ frozen ground observations

To ensure the validity of the model, we collected daily data from the frozen ground stations located in the UYRB, including three seasonally frozen ground stations (CST_01, NST_03, and ELH) and one permafrost station (CLP) (Fig. 1b). Stations CST_01 and NST_03 are located near the Maqu meteorological station in the southeastern part of the UYRB and recorded soil temperature and soil moisture data for the 5 cm soil depth layer⁴⁰. Station ELH is located on the north side of Ngöring Lake and recorded soil temperature profiles for eight soil layers. Station CLP is located in Chalaping and recorded soil temperature profiles and soil moisture profiles for 10 soil layers^{34,35,41}.

The simulation results show that the 5 cm soil temperature at site CST_01 had a BIAS of -0.21 °C and an RMSE of -2.34 °C. Similarly, the simulated 5 cm soil temperature at NST_03 had a BIAS of -0.31 °C and an RMSE of -2.97 °C. The simulation of the soil temperature profile at site ELH was accurate and effectively captured the initial thawing and freezing of each soil layer. The simulation results for CLP site can depict the zero-curtain process, and the simulated ALT is similar to the observed value.

Regarding soil moisture, the simulated 5-cm soil moisture at site CST_01 has a BIAS of 0.019 m³m⁻³ and an RMSE of 0.094 m³m⁻³, while the 5-cm soil moisture at NST_03 has a BIAS of -0.025 m³m⁻³ and an RMSE of 0.077 m³m⁻³. The simulated soil moisture at CLP is lower than observed above the active layer, but higher than observed below the active layer. This discrepancy may be due to an underestimation of soil porosity in the simulation.

To enhance computational efficiency and accuracy, we utilized the inverse distance weighted interpolation method to spatially integrate the climate forcing data. This unified the data to a spatial resolution of 5 km.

Model description

In this study, the model water and energy budget-based distributed hydrological model permafrost version (WEB-DHM-pf) was utilized^{36,42}.

This model is based on the WEB-DHM model^{13–46} that takes into account the phase transitions within the unconfined aquifer and the interaction of the overlying soil.

This model employs enthalpy instead of the soil temperature as a forecasting variable to decrease the uncertainty in the release of latent heat caused by the phase change from water to ice on the soil temperature and soil moisture. Using enthalpies contributes to energy conservation and enables us to characterize the continuous, slow changes in the energy throughout the soil layers^{46,47}. By using enthalpy as a predictive variable, the model can overcome the inaccuracies and discontinuities caused by the ice-water phase transition in the traditional soil temperature approach, thus improving the precision and stability of the simulation results. Additionally, the WEB-DHM-pf model considers the initial boundary conditions of the bottom layer of soil (above the unconfined aquifer). In addition to soil temperature and moisture, the model incorporates ground ice to improve the characterization of the hydrological processes in the permafrost layer.

The model was constructed using DEM data from subsection 5.1 to calculate watershed division, slope length, and angle. Additionally, static data on soil organic carbon in the soil layer from 0 to 200 cm, soil type, and land use were considered. Finally, the model was completed by incorporating meteorological and vegetation dynamic data. The model parameters for the soil anisotropy coefficient, saturated hydraulic conductivity of the unconfined aquifer layer, surface soil, and deep soil, as well as Van Genuchten's equation, were calibrated to simulate changes in daily runoff in the watershed. For more information on the specific algorithms, parameter settings, and application of the model in simulating permafrost hydrology, please refer to Song et al.^{36,42}.

Data availability

The data used in this paper and their available sources are as follows. The DEM was provided by NASA (<http://srtm.csi.cgiar.org/>), the meteorological data were provided by the China Meteorological Administration (<http://data.cma.cn/en/?r=data/detail&dataCode=A.0012.0001>), the land use data were provided by the USGS (<https://www.usgs.gov/media/images/glcc-global-composite>), the soil type data were provided by the FAO (<http://www.fao.org/soils-portal/soil-survey/soil-maps-and-databases/other-global-soil-maps-and-databases/en/>), the soil organic carbon data were obtained from SoilGrids (https://soilgrids.org/#/?layer¼ORCDRC_M_sl2_250m%26;vector¼1), and the soil moisture and temperature data were provided by the NTPDC (<https://data.tpdac.cn/en/data/ef949bb0-26d4-4cb6-acc2-3385413b91ee/>). The vegetation data can be accessed at <http://www.glass.umd.edu/Download.html>. The derived data supporting the findings of this study are available from the corresponding author upon reasonable request.

Code availability

The source codes for the analysis of this study are available from the corresponding author upon reasonable request.

Received: 14 December 2023; Accepted: 22 February 2024;

Published online: 02 March 2024

References

1. Zhang, Y. S., Ohata, T. & Kadota, T. Land-surface hydrological processes in the permafrost region of the eastern Tibetan Plateau. *J. Hydrol.* **283**, 41–56 (2003).
2. Ding, Y. J. & Xiao, C. D. Challenges in the study of cryospheric changes and their impacts (in Chinese). *Adv. Earth Sci.* **28**, 1067–1076 (2013).
3. Dobinski, W. Permafrost. *Earth Sci. Rev.* **108**, 158–169 (2011).
4. Hu, G. et al. Spatiotemporal variations and regional differences in air temperature in the permafrost regions in the Northern Hemisphere during 1980–2018. *Sci. Total Environ.* **791**, 148358 (2021).

5. Everdingen, R. V. *Glossary of Permafrost and Related Ground-ice Terms*. Technical Memorandum No. 142 (National Research Council of Canada, 1998).
6. Wu, Q. B. & Zhang, T. J. Recent permafrost warming on the Qinghai-Tibetan Plateau. *J. Geophys. Res. Atmos.* **113**, 133675 (2008).
7. Zou, D. F. et al. A new map of permafrost distribution on the Tibetan Plateau. *Cryosphere* **11**, 2527–2542 (2017).
8. Ran, Y., Li, X. & Cheng, G. Climate warming over the past half century has led to thermal degradation of permafrost on the Qinghai-Tibet Plateau. *Cryosphere* **12**, 595–608 (2018).
9. Guo, D. & Wang, H. The significant climate warming in the northern Tibetan Plateau and its possible causes. *Int. J. Climatol.* **32**, 1775–1781 (2011).
10. Wang, G. X., Liu, G. S. & Liu, L. A. Spatial scale effect on seasonal streamflows in permafrost catchments on the Qinghai-Tibet Plateau. *Hydrol. Process.* **26**, 973–984 (2012).
11. Cheng, G. D. & Jin, H. J. Groundwater in the permafrost regions on the Qinghai-Tibet Plateau and it changes (in Chinese). *Hydrogeol. Eng. Geol.* **40**, 11 (2013).
12. Niu, L. et al. Effect of permafrost degradation on hydrological processes in typical basins with various permafrost coverage in Western China. *Sci. China Earth Sci.* **54**, 615–624 (2011).
13. Hu, G. et al. Thermal properties of active layer in permafrost regions with different vegetation types on the Qinghai-Tibetan Plateau. *Theor. Appl. Climatol.* **139**, 983–993 (2020).
14. Gao, B. et al. Change in frozen soils and its effect on regional hydrology, upper Heihe basin, northeastern Qinghai-Tibetan Plateau. *Cryosphere* **12**, 657–673 (2018).
15. Wang, T. et al. Pervasive permafrost thaw exacerbates future risk of water shortage across the Tibetan Plateau. *Earth's Future* **11**, e2022EF003463 (2023a).
16. Wang, T. et al. Unsustainable water supply from thawing permafrost on the Tibetan Plateau in a changing climate. *Sci. Bull.* **68**, 1105–1108 (2023b).
17. Guo, D. & Wang, H. Simulation of permafrost and seasonally frozen ground conditions on the Tibetan Plateau, 1981–2010. *J. Geophys. Res. Atmos.* **118**, 5216–5230 (2013).
18. Su, Y. et al. Remotely sensed lake area changes in permafrost regions of the Arctic and the Tibetan Plateau between 1987 and 2017. *Sci. Total Environ.* **880**, 163355 (2023).
19. Luo, J. et al. The characteristics and patterns of retrogressive thaw slumps developed in permafrost region of the Qinghai-Tibet Plateau (in Chinese). *J. Glaciol. Geocryol.* **44**, 96–105 (2022).
20. Qin, Y. et al. Impacts of climate warming on the frozen ground and eco-hydrology in the Yellow River source region, China. *Sci. Total Environ.* **605**, 830–841 (2017).
21. Cao, B., Li, X., Feng, M. & Zheng, D. Quantifying overestimated permafrost extent driven by rock glacier inventory. *Geophys. Res. Lett.* **48**, e2021GL092476 (2021).
22. Wu, T. et al. Weakening of carbon sink on the Qinghai-Tibet Plateau. *Geoderma* **412**, 115707 (2022).
23. Jones, B. M. et al. Lake and drained lake basin systems in lowland permafrost regions. *Nat. Rev. Earth Environ.* **3**, 85–98 (2022).
24. Zhuang, Q. et al. Carbon dynamics of terrestrial ecosystems on the Tibetan Plateau during the 20th century: an analysis with a process-based biogeochemical model. *Glob. Ecol. Biogeogr.* **19**, 649–662 (2010).
25. Mu, C. et al. The status and stability of permafrost carbon on the Tibetan Plateau. *Earth Sci. Rev.* **211**, 103433 (2020).
26. Zhang, Y. et al. Coupling of a simultaneous heat and water model with a distributed hydrological model and evaluation of the combined model in a cold region watershed. *Hydrol. Process* **27**, 3762–3776 (2013).
27. Cheng, G. D. et al. Characteristic, changes and impacts of permafrost on Qinghai-Tibet Plateau (in Chinese). *Chin. Sci. Bull.* **64**, 2783–2795 (2019).
28. Tang, Q. H. et al. Streamflow change on the Qinghai-Tibet Plateau and its impacts (in Chinese). *Chin. Sci. Bull.* **64**, 2807–2821 (2019).
29. Gao, S. Q. et al. Analysis of vegetation coverage changes and natural driving forces of spatial distribution in the source region of the Yellow River (in Chinese). *Ecol. Environ. Sci.* **31**, 429–439 (2022).
30. Kang, Y. et al. Trend of vegetation evaluation and its responses to climate change over the source region of the yellow river (in Chinese). *Clim. Environ. Res.* **16**, 505–512 (2011).
31. Wang, Y., Li, Y. H. & Sun, X. Y. Impact of climate change on the eco-environment in the Yellow River Source (in Chinese). *Pratacultural Sci.* **32**, 539–551 (2015).
32. Jin, H. et al. Changes in frozen ground in the Source Area of the Yellow River on the Qinghai-Tibet Plateau, China, and their eco-environmental impacts. *Environ. Res. Lett.* **4**, 045206 (2009).
33. Zhang, Q., Xu, C. Y. & Yang, T. Variability of water resource in the Yellow River basin of past 50 years, China. *Water Resour. Manag.* **23**, 1157–1170 (2009).
34. Luo, D. et al. Spatiotemporal characteristics of freezing and thawing of the active layer in the source areas of the Yellow River (SAYR). *Chin. Sci. Bull.* **59**, 3034–3045 (2014).
35. Luo, D. et al. Characteristics of ground surface temperature at Chalaping in the Source Area of the Yellow River, northeastern Tibetan Plateau. *Agric. Meteorol.* **281**, 107819 (2020).
36. Song, L. et al. Divergent runoff impacts of permafrost and seasonally frozen ground at a large river basin of Tibetan Plateau during 1960–2019. *Environ. Res. Lett.* **17**, 124038 (2022).
37. Zhao, X. et al. The Global Land Surface Satellite (GLASS) remote sensing data processing system and products. *Remote Sens.* **5**, 2436–2450 (2013).
38. Yang, K., Huang, G. W. & Tamai, N. A hybrid model for estimating global solar radiation. *Sol. Energy* **70**, 13–22 (2001).
39. Yang, K., Koike, T. & Ye, B. Improving estimation of hourly, daily, and monthly solar radiation by importing global data sets. *Agric. Meteorol.* **137**, 43–55 (2006).
40. Su, Z. B. et al. The Tibetan Plateau observatory of plateau scale soil moisture and soil temperature (Tibet-Obs) for quantifying uncertainties in coarse resolution satellite and model products. *Hydrol. Earth Syst. Sci.* **15**, 2303–2316 (2011).
41. Luo et al. Thermal regime of warm-dry permafrost in relation to ground surface temperature in the Source Areas of the Yangtze and Yellow rivers on the Qinghai-Tibet Plateau, SW China. *Sci. Total Environ.* **618**, 1033–1045 (2018).
42. Song, L. et al. Improving permafrost physics in a distributed cryosphere-hydrology model and its evaluations at the upper Yellow River basin. *J. Geophys. Res. Atmos.* **125**, e2020JD032916 (2020).
43. Wang, L. et al. Assessment of a distributed biosphere hydrological model against streamflow and MODIS land surface temperature in the upper Tone River Basin. *J. Hydrol.* **377**, 21–34 (2009).
44. Wang, L. et al. Frozen soil parameterization in a distributed biosphere hydrological model. *Hydrol. Earth Syst. Sci.* **14**, 557–571 (2010).
45. Wang, L. et al. Improving snow process modeling with satellite-based estimation of near-surface-air-temperature lapse rate. *J. Geophys. Res. Atmos.* **121**, 12,005–12,030 (2016).
46. Wang, L. et al. Development of a land surface model with coupled snow and frozen soil physics. *Water Resour. Res.* **53**, 5085–5103 (2017).
47. Bao, H. et al. Development of an enthalpy-based frozen soil model and its validation in a cold region in China. *J. Geophys. Res. Atmos.* **121**, 5259–5280 (2016).

Acknowledgements

This research was financially supported by the Second Tibetan Plateau Scientific Expedition and Research Program (grant 2019QZKK020604), and the National Natural Science Foundation of China (Grant No. 92047301 and 41988101).

Author contributions

S.L. and W.L. conceived and designed the study. S.L. performed the analyses, and wrote the manuscript. W.L. provided the original architecture for WEB-DHM. L.D. provided the in-situ observations. All the co-authors revised the manuscript. W.L. and C.D. acquired project funds.

Competing interests

The authors declare no competing interests.

Additional information

Supplementary information The online version contains supplementary material available at

<https://doi.org/10.1038/s41612-024-00607-3>.

Correspondence and requests for materials should be addressed to Lei Wang.

Reprints and permissions information is available at

<http://www.nature.com/reprints>

Publisher's note Springer Nature remains neutral with regard to jurisdictional claims in published maps and institutional affiliations.

Open Access This article is licensed under a Creative Commons Attribution 4.0 International License, which permits use, sharing, adaptation, distribution and reproduction in any medium or format, as long as you give appropriate credit to the original author(s) and the source, provide a link to the Creative Commons licence, and indicate if changes were made. The images or other third party material in this article are included in the article's Creative Commons licence, unless indicated otherwise in a credit line to the material. If material is not included in the article's Creative Commons licence and your intended use is not permitted by statutory regulation or exceeds the permitted use, you will need to obtain permission directly from the copyright holder. To view a copy of this licence, visit <http://creativecommons.org/licenses/by/4.0/>.

© The Author(s) 2024